Peregrine rogue waves induced by the interaction between a continuous wave and a soliton

Guangye Yang, Lu Li, and Suotang Jia

Phys. Rev. E **85**, 046608 — Published 26 April 2012

DOI: 10.1103/PhysRevE.85.046608

The Peregrine rogue waves induced by interaction between the continuous wave and soliton

Guangye Yang[1,2], Lu Li[1*] and Suotang Jia[3]
[1] *Institute of Theoretical Physics, Shanxi University, Taiyuan, Shanxi, 030006, China*
[2] *Department of physics, Shanxi Medical University, Taiyuan, Shanxi, 030001, China and*
[3] *College of physics and Electronics Engineering, Shanxi University, Taiyuan 030006, China*

Based on the soliton solution on a continuous wave background for integrable Hirota equation, the reduction mechanism and the characteristics of the Peregrine rogue wave in the propagation of femtosecond pulses of optical fiber are discussed. The results show that there exist two processes of the formation of the Peregrine rogue wave, one is the localized process of CW background, other is the reduction process of the periodization of the bright soliton. The characteristics of the Peregrine rogue wave is exhibited by strong temporal and spatial localization. Also, various initial excitations of the Peregrine rogue wave are performed and the results show that the Peregrine rogue wave can be excited by a small localized (single peak) perturbation pulse of the continuous wave background, even for the nonintegrable case. The numerical simulations show that the Peregrine rogue wave is unstable. Finally, through a realistic example, the influence of the self-frequency shift to the dynamics of the Peregrine rogue wave is discussed. The results show that, in the absence of the self-frequency shift, the Peregrine rogue wave can splits into several subpusles, however, when the self-frequency shift is considered, the Peregrine rogue wave no longer splits, and exhibits mainly a peak changing and increasing evolution property of the field amplitude.

PACS numbers: 42.65.Tg, 42.81.Dp, 42.79.Sz

I. INTRODUCTION

Rogue wave is an oceanic phenomenon with amplitude much higher than the average wave crests around them [1]. So far, this phenomenon has not been understood completely due to the difficult and restricted observational conditions. Therefore, a great deal of attentions have been paid to understand better their physical mechanisms, and suggested that the rogue waves appeared in the ocean were mainly caused by the wave-wave nonlinear interaction, such as modulation instability of the Benjamin-Feir-type [2–6]. Recently, the rogue waves have been observed in optical fibers [7], in superfluid helium [8], and in capillary waves [9], respectively. These discoveries indicate that the rogue waves may be rather universal. Certainly, we do not expect the occurrence of the rogue waves in the ocean due to its enormous destructiveness. In optics, however, the optical rogue waves produced in supercontinuum generation can be used to generate highly energetic optical pulses [7, 10–13].

The deep waves in ocean and the wave propagation in optical fibers can be described by the nonlinear Schrödinger (NLS) equation. Based on the model, the rogue wave phenomenon have been extensively studied, including rational solutions and their interactions [14–21], pulse splitting induced by higher-order modulation instability and wave turbulence [22, 23]. A fundamental analytical solution on the rogue waves is Peregrine solution (PS) which was first presented by Peregrine [24]. PS is a localized solution in both time and space, and is a limiting case of Kuznetsov-Ma solitons [25, 26] and Akhmediev breathers [27]. Recently, the excitation conditions of PS have been demonstrated experimentally in optical fiber, and explicitly characterized its two-dimensional localization [28, 29]. It should be noted that the results are theoretically described by NLS equation, which is valid for the picosecond pulses. When describing the characteristics of PS in the femtosecond regime, we must consider some higher-order effects, such as third-order dispersion (TOD), self-steepening and self-frequency shift and so on. In this case, we should consider the higher-order nonlinear Schrödinger (HNLS) equation in the form [30]

$$\frac{\partial q}{\partial z} = i\left(\alpha_1 \frac{\partial^2 q}{\partial t^2} + \alpha_2 |q|^2 q\right) + \alpha_3 \frac{\partial^3 q}{\partial t^3} + \alpha_4 \frac{\partial |q|^2 q}{\partial t} + \alpha_5 q \frac{\partial |q|^2}{\partial t}, \quad (1)$$

where $q(z,t)$ is the slowly varying envelope of the electric field, z and t denote normalized propagation distance and retarded temporal coordinate, respectively, and the parameters $\alpha_1, \alpha_2, \alpha_3, \alpha_4$ and α_5 are the real constants related to the group velocity dispersion (GVD), the self-phase modulation (SPM), the third-order dispersion (TOD), the self-steepening and the delayed nonlinear response effect, respectively.

Generally, the HNLS equation (1) is not integrable. To solve the equation (1), we first consider the special parametric choice with $\alpha_2 = 2\mu^2\alpha_1$, $\alpha_4 = 6\mu^2\alpha_3$, $\alpha_4 + \alpha_5 = 0$ so that Eq. (1) becomes [31]

$$\frac{\partial q}{\partial z} = i\left(\alpha_1 \frac{\partial^2 q}{\partial t^2} + \alpha_2 |q|^2 q\right) + \alpha_3 \frac{\partial^3 q}{\partial t^3} + \alpha_4 |q|^2 \frac{\partial q}{\partial t}, \quad (2)$$

*Electronic address: llz@sxu.edu.cn

which is usually called the Hirota equation, where the parameter μ is a real constant.

The equation was first presented by Hirota [31], and subsequently many researchers analyzed this equation from different points of view [32–39]. Recently, the rogue waves and the rational solutions of the Hirota equation have been discussed in the forms of the two lower-order solutions by employing the Darboux transformation technique [40]. In this paper, based on the soliton solution on a continuous wave (CW) background for integrable Hirota equation (2), we discuss the formation mechanism and the characteristics of the PS in the femtosecond regime. The results show that the PS exhibits a feature of temporal and spatial localization and can be excited by a small localized (single peak) perturbation pulse of CW background even for nonintegrable HNLS equation (1). Based on the result, we discuss the dynamics of the Peregrine rogue wave through a realistic example.

The paper is organized as follows. In Sec. II, we present explicit process of the formation of the PS from the Kuznetsov-Ma solitons and Akhmediev breathers based on the soliton solution on a continuous wave (CW) background for Hirota equation and discuss the characteristics of the PS. Various initial excitations of the PS are discussed in Sec. III. Subsequently, in Sec. IV, we investigate the influence of the self-frequency shift to the dynamics of the Peregrine rogue wave by employing a realistic example. Our results are summarized in Sec. IV.

II. THE PEREGRINE SOLUTION INDUCED BY INTERACTION BETWEEN THE CONTINUOUS WAVE BACKGROUND AND SOLITON

By employing Darboux transformation, one can construct the soliton solution on a continuous wave background for Eq. (2) as follows [38, 39]

$$q(z,t)=\left(A+A_s\frac{a\cosh\theta+\cos\varphi}{\cosh\theta+a\cos\varphi}+iA_s\frac{b\sinh\theta+c\sin\varphi}{\cosh\theta+a\cos\varphi}\right)\exp\left(i\varphi_c\right). \tag{3}$$

Here

$$\begin{aligned}\theta&=M_IT-\left(\nu_1M_R+\nu_2M_I\right)Z,\\ \varphi&=M_RT-\left(\nu_2M_R-\nu_1M_I\right)Z,\\ \varphi_c&=\omega T+\left[(2\mu^2A^2-\omega^2)\alpha_1+\omega(6\mu^2A^2-\omega^2)\alpha_3\right]Z,\end{aligned}$$

with $T=t-t_0$, $Z=z-z_0$, and the coefficients are $a=-2\mu^2AA_s/(\mu^2A_s^2+M_R^2)$, $b=-2\mu AM_R/(\mu^2A_s^2+M_R^2)$, and $c=M_I/(\mu A_s)$, which implies that $M_I=0$ as $A_s=0$. And other coefficients $\nu_1=\mu A_s[\alpha_1+(\omega+2\omega_s)\alpha_3]$, $\nu_2=(\omega+\omega_s)\alpha_1+(\omega^2+\omega\omega_s+\omega_s^2-2\mu^2A^2-\mu^2A_s^2)\alpha_3$, $M_R=\{[((\omega_s-\omega)^2+4\mu^2A^2-\mu^2A_s^2)^2+4\mu^2A_s^2(\omega_s-\omega)^2]^{1/2}+((\omega_s-\omega)^2+4\mu^2A^2-\mu^2A_s^2)\}^{1/2}/\sqrt{2}$, and $M_I=\{[((\omega_s-\omega)^2+4\mu^2A^2-\mu^2A_s^2)^2+4\mu^2A_s^2(\omega_s-\omega)^2]^{1/2}-((\omega_s-\omega)^2+4\mu^2A^2-\mu^2A_s^2)\}^{1/2}/\sqrt{2}$, and t_0, z_0, A, ω, A_s, and ω_s are the arbitrary real constants, and without loss of generality we assume that A and A_s are non-negative constants. The solution (3) includes two special cases. One is that as the amplitude A vanishes, it reduces to the solution $q_s(z,t)=A_se^{i\varphi_s}\operatorname{sech}\theta$, where $\theta=\mu A_sT-\mu A_s[2\omega_s\alpha_1+(3\omega_s^2-\mu^2A_s^2)\alpha_3]Z$ and $\varphi_s=\varphi_c+\varphi=\omega_sT+\left[\left(\mu^2A_s^2-\omega_s^2\right)\alpha_1+\omega_s(3\mu^2A_s^2-\omega_s^2)\alpha_3\right]Z$, which describes a bright soliton solution with the maximal amplitude A_s. The other is that when the soliton amplitude A_s vanishes, it reduces to the continuous wave (CW) light solution $q_c(z,t)=Ae^{i\varphi_c}$. Therefore, in general, the exact solution $q(z,t)$ in Eq. (3) describes a soliton solution embedded in a CW light background with the group velocity $V_{sc}=(\nu_1M_R+\nu_2M_I)/M_I$ [39]. Especially, when $\alpha_3=0$ and taking $\alpha_1=-1$, $\mu=1$, the solution (3) coincides with the result given in Ref. [41], which is firstly derived from NLS equation by N. Akhmediev and V. I. Korneev [27].

In the limit $(A_s,\omega_s)\to(2A,\omega)$, Eq. (3) reduces to PS as follows

$$q_{\mathrm{p}}(z,t)=Ae^{i\varphi_c}\left[\frac{4+i8CZ}{1+4C^2Z^2+4B^2\left(T-DZ\right)^2}-1\right], \tag{4}$$

where $B=\mu A$, $C=2B^2(\alpha_1+3\omega\alpha_3)$ and $D=2\omega\alpha_1+3(\omega^2-2B^2)\alpha_3$, which is a rational fraction solution, and is firstly derived from Kuznetsov-Ma Breather (KMB) by H. Peregrine [24–26] and so is called the Peregrine solution or the Peregrine rogue wave (note that it is regarded as the Peregrine soliton in Refs. [28, 29]). Here (t_0,z_0) presents the peak position of the PS. In order to understand the characteristics of the solution (3), Figure 1 presents the reduced process from the solutions (3) to the PS (4) as $(A_s,\omega_s)\to(2A^-,\omega)$ and $(A_s,\omega_s)\to(2A^+,\omega)$, respectively. From them one can see directly that the solution (3) commonly exhibits a breather characteristics, and the separation between adjacent peaks gradually increases as $(A_s,\omega_s)\to(2A,\omega)$, eventually reduces into the PS. The most impressive feature on the PS is localized in both time and space. The peak position of the PS is fixed at spatio-temporal position $z=z_0$ and $t=t_0$ during the reduction, and the peak power $|q_{\mathrm{p}}(z_0,t_0)|^2=(A+A_s)^2\to 9A^2$ as $A_s\to 2A$, which means that the PS with peak power $9A^2$ can be generated by choosing an initial excitation properly.

It should be pointed out that in the reduction process mentioned above, the physical mechanism for the formation of the PS has some differences. Figs. 1(a$^-$)-(e) demonstrate a localized process of CW background along the slope direction $K_\varphi=M_R/(\nu_2M_R-\nu_1M_I)$, while Figs. 1(a$^+$)-(e) show a periodization process of bright soliton along the slope direction $K_\theta=M_I/(\nu_1M_R+\nu_2M_I)$. Furthermore, Figure 2 presents the contour plots of K_θ and K_φ as a function of A_s and ω_s for given A and ω. Note that K_φ is infinite as $\nu_2M_R-\nu_1M_I=0$ except for the point $(2A,\omega)$, which corresponds to the line $t=t_0$ and appears at the sixth curve in Fig. 2(b). When $(A_s,\omega_s)\to(2A,\omega)$, the limitations of K_φ and K_θ do not

exist, and at this point the solution is localized along both slope directions K_φ and K_θ, namely, the PS appears. Therefore, the PS should be a middle state in the process of the localization of CW converting into the periodization of the bright soliton, as shown in Ref. [17].

In order to understand better the reduction processes of the PS, we consider a especial case for the solution (3) with $\omega_s = \omega$. In this case, the solution (3) has two different expressions. When $A_s^2 < 4A^2$, the solution (3) can be written as

$$q(z,t) = \left(\Omega_R \frac{\Omega_R \cosh\theta + iA_s \sinh\theta}{2A\cosh\theta - A_s\cos\varphi} - A\right) e^{i\varphi_c}, \quad (5)$$

where $\theta = \mu^2 A_s \Omega_R(\alpha_1 + 3\omega\alpha_3)Z$ and $\varphi = \mu\Omega_R T - \mu\Omega_R[2\omega\alpha_1 + (3\omega^2 - 2\mu^2A^2 - \mu^2A_s^2)\alpha_3]Z$ with $\Omega_R = \sqrt{4A^2 - A_s^2}$ being a modulation frequency. Here $K_\theta = 0$ and $K_\varphi = 1/[2\omega\alpha_1 + (3\omega^2 - 2\mu^2A^2 - \mu^2A_s^2)\alpha_3]$. Therefore, the solution (5) is periodic with period $t_{\rm per} = 2\pi/(\mu\Omega_R)$ along the t axis and localized along the z axis, and is usually called Akhmediev breather (AB), which can be considered as a modulation instability process [42]. In this case, the solution (5) can reduce to the CW background $q_c(z,t)$ as $A_s \to 0$, and with the increasing of A_s the CW background is gradually localized due to the interaction with the soliton and forms a periodic breather with period $t_{\rm per}$, i. e. Akhmediev breather (AB) [see Fig. 3(a)], eventually when A_s tends to $2A$, the solution (5) becomes the PS. This process represents the reduction of CW→AB→PS. Also, it can be described by the ratio between the period $t_{\rm per}$ and the temporal width δt_0 as follows

$$\frac{t_{\rm per}}{\delta t_0} = \frac{2\pi}{\cos^{-1}\left(\frac{A_s}{A} - 2\frac{A}{A_s}\right)}, \quad (6)$$

where the temporal width δt_0 is defined as the width from zero-valued of intensity to adjacent peak [28]. Figure 3(b) presents the dependence of the ratio $t_{\rm per}/\delta t_0$ on A_s/A. From it, one can see that when A_s/A approaches to 2, the ratio $t_{\rm per}/\delta t_0$ tends to infinity, which implies that the separation between peaks is more and more larger, eventually results in the localization along the t axis, and forms the PS. From the expression (6), one can see that this process does not depend on the higher-order parameter α_3, which means that when the higher-order effects with the conditions $\alpha_2 = 2\mu^2\alpha_1$, $\alpha_4 = 6\mu^2\alpha_3$, and $\alpha_4 + \alpha_5 = 0$ simultaneously appear in optical fiber, they do not influence the characteristics of the PS. It should be emphasized that the Peregrine solution generated by the process of the reduction of CW→AB→PS has been already studied theoretically and experimentally in the framework of NLS equation [14, 17, 26–29], here we presented the corresponding descriptions in the femtosecond regime.

When $A_s^2 > 4A^2$, the solution (3) can reduce to the following form

$$q(z,t) = \left(\Omega_I \frac{\Omega_I \cos\varphi + iA_s \sin\varphi}{A_s\cosh\theta - 2A\cos\varphi} - A\right) e^{i\varphi_c}, \quad (7)$$

where $\theta = \mu\Omega_I T - \mu\Omega_I[2\omega\alpha_1 + (3\omega^2 - 2\mu^2A^2 - \mu^2A_s^2)\alpha_3]Z$ and $\varphi = \mu^2 A_s\Omega_I(\alpha_1 + 3\omega\alpha_3)Z$ with $\Omega_I = \sqrt{A_s^2 - 4A^2}$. Here $K_\theta = 1/[2\omega\alpha_1 + (3\omega^2 - 2\mu^2A^2 - \mu^2A_s^2)\alpha_3]$ and $K_\varphi = 0$. Especially as $A_s \gg 2A$, namely $\Omega_I \sim A_s$, the solution (7) can be approximated as $q(z,t) \approx q_s(z,t) - q_c(z,t)$, which is the superposition of a CW solution and a bright soliton with the larger amplitude A_s. From the solution (7), one can see that it is a periodic function with period $z_{\rm per} = 2\pi/\mu^2 A_s\Omega_I(\alpha_1 + 3\omega\alpha_3)$ along the z axis and is localized along the t axis, and possesses the periodic peaking property of the field amplitude like Kuznetsov-Ma soliton (KMS) [25, 26, 38], and so is usually called Kuznetsov-Ma soliton, as shown in Fig. 3(c). In this case, the solution (7) can reduce to the bright soliton $q_s(z,t)$ as $A \to 0$, and with the increasing of A, the bright soliton is periodized due to the interaction with CW background and forms a Kuznetsov-Ma soliton (KMS), eventually reduces into the PS. This process represents the reduction of bright soliton→KMS→PS. Similarly, this process can be described by the ratio between the period $z_{\rm per} = 2\pi/\mu^2 A_s\Omega_I(\alpha_1 + 3\omega\alpha_3)$ and δz_0 in the form

$$\frac{z_{\rm per}}{\delta z_0} = \frac{\pi}{\cos^{-1}\left[\frac{A_s(-7A^2 - 2AA_s + A_s^2)}{2A(A^2 - 2AA_s - A_s^2)}\right]}, \quad (8)$$

where δz_0 is defined as the distance between two corresponding locations of half of the peak intensity along the slope direction K_θ. Figure 3(d) presents the dependence of the ratio $z_{\rm per}/\delta z_0$ on A_s/A. From it, one can see that when A_s/A approaches to 2, the ratio $z_{\rm per}/\delta z_0$ tends to infinity, which means that the distance between peaks is more and more larger, eventually results in the formation of the PS. Similarly, the expression (8) does not depend on the parameter α_3.

Another feature of PS can be described by the z-independent integral and the energy exchange between the PS and the CW background. Indeed, by introducing the light intensity against the CW background as follows

$$\begin{aligned} E_c(t,z) &= |q_p(t,z)|^2 - |q_p(\pm\infty,z)|^2 \\ &= A^2 \frac{8 + 32C^2Z^2 - 32B^2(T - DZ)^2}{[1 + 4C^2Z^2 + 4B^2(T - DZ)^2]^2}, \end{aligned} \quad (9)$$

it can be shown that it possesses the z-independent integral property, i. e. $\int_{-\infty}^{+\infty} E_c(t,z)dt = 0$. From the condition $E_c(t_0 \pm 1/2B, z_0) = 0$, one can define the width of PS as $1/B$, and have integrals $\int_{-1/2B}^{+1/2B} E_c(t,z_0)dt = 4A^2/B$ and $\int_{-\infty}^{-1/2B} E_c(t,z_0)dt + \int_{+1/2B}^{\infty} E_c(t,z_0)dt = -4A^2/B$. These results show that the energy of PS with stronger intensity mainly concentrates in its central interval $(-1/2B, 1/2B)$, but as a result of z-independent integral property, it loses the same energy in the background so that the relation $S_1 + S_2 = S_3$ hold, as shown in Figs. 4(a)-4(c). It should be noted that because $B = \mu A$ is independence of the higher-order terms in Eq. (2), the higher-order effects do not influence this property on the PS.

The energy exchange between the PS and the CW background is of the form

$$E_e(z) = \int_{-\infty}^{+\infty} |q_p(t,z) - q_p(\pm\infty, z)|^2 \, dt = \frac{4A^2\pi}{B\sqrt{1+4[2B^2(\alpha_1+3\omega\alpha_3)]Z^2}}. \quad (10)$$

From the expression (10), one can see that $E_e(z)$ is aperiodic function of z, which differs from the periodic exchange between the bright soliton and the CW background in Eq. (3) [39]. Also, one find that $E_e(z)$ is monotonously increasing as $z < z_0$ and is monotonously decreasing as $z > z_0$, thus it takes maximal value at $z = z_0$, as shown in Fig. 4(d). This result shows that at $z = z_0$ the energy exchange between the PS and the CW background reaches maximum. In order to understand the influence of the higher-order effects on the PS, Figure 4(d) presents the evolution plots of $E_e(z)$ for different TOD parameter α_3. From it, one can see that the increase of the TOD parameter α_3 can enhance the rate of the energy exchange, as shown in Figs. 4(a) and 4(b).

III. INITIAL EXCITATIONS OF THE PEREGRINE ROGUE WAVES

In this Section, we will discuss the initial excitations of the Peregrine rogue wave. We start with considering the excitation of the Peregrine rogue wave based on the solutions (5) and (7). For the solution (5), linearizing its initial expression, one find that the initial expression of the solution (5) can be approximated by

$$q_\pm(0,t) \approx (\rho_\pm + \epsilon_\pm \cos\varphi)\, e^{i\varphi_c(0,t)}, \quad (11)$$

where $\rho_\pm = (2A^2 - A_s^2 \mp iA_s\Omega_R)/(2A)$ with $|\rho_\pm| = A$, $\epsilon_\pm = A_s\Omega_R(\Omega_R \mp iA_s)/(2A^2)\exp[\mp\mu^2 A_s(\alpha_1 + 3\omega\alpha_3)\Omega_R z_0]$, and $\varphi = \mu\Omega_R T + \mu\Omega_R[2\omega\alpha_1 + (3\omega^2 - 2\mu^2A^2 - \mu^2A_s^2)\alpha_3]z_0$. Here the subscripts "+" and "−" correspond to the case of $\alpha_1+3\omega\alpha_3 > 0$ and $\alpha_1+3\omega\alpha_3 < 0$, respectively. It can be shown that $\epsilon_\pm \to 0$ as $A_s \to 2A$. Thus, the expression (11) can is regarded as an initial condition with a small periodic perturbation of background with the period $t_{\rm per}$. The numerical simulations show that the evolution of the exact solution (5) can be well described by the initial approximation (11) (also see Ref. [39]). Here one make use of the initial approximation (11) to excite the Peregrine rogue wave as A_s closes to $2A$.

Figure 5 presents the evolution plots of the numerical solution of Eq. (2) with the initial condition (11) and the comparisons of the intensity profile between numerical and exact Peregrine rogue waves at peak position for $\alpha_3 = 0$ and $\alpha_3 \neq 0$, respectively. From it, one can see that when A_s approaches to $2A$, the initial condition (11) evolves into a string of near-ideal Peregrine rogue waves. Although the theoretical results reveal that there only is a Peregrine rogue wave in the limitation of $A_s \to 2A$, in practice, this can not implement due to $\epsilon_\pm = 0$ as $A_s = 2A$. Furthermore, from Figs. 5(a) and 5(b), it can be seen that the evolution for long distance shows the breakup of the Peregrine rogue wave, which implies that the Peregrine rogue wave is unstable. Also, from Figs. 5(c) and 5(d), one can see that the presence of the higher-order effects did not markedly influence the intensity distribution of the Peregrine rogue wave at peak position except for a displacement of the peak position, but shorten the distance of energy exchange, as shown in Figs. 5(a) and 5(b). This is agreement with that suggested in Fig. 4(d).

In the following, we discuss the initial excitation induced by the solution (7). In this case, one find that the solution (7) can take the following particular form

$$q(z_1,t) = (-A + i\Omega_I \operatorname{sech}\theta)\, e^{i\varphi_c(z_1,t)} = Ae^{i[\varphi_c(z_1,t)+\pi]} + \Omega_I \operatorname{sech}\theta e^{i\left[\varphi_c(z_1,t)+\frac{\pi}{2}\right]} \quad (12)$$

at the location $z_1 = (2n\pi+\pi/2)/[\mu^2A_s\Omega_I(\alpha_1+3\omega\alpha_3)] + z_0$, $n = 0, \pm1, \pm2, \cdots$, where $\theta = \mu\Omega_I T - [2\omega\alpha_1 + (3\omega^2 - 2\mu^2A^2 - \mu^2A_s^2)\alpha_3](2n\pi+\pi/2)/[\mu A_s(\alpha_1+3\omega\alpha_3)]$. Without loss of generality, here we take $n = 0$. The expression (12) is the superposition of a CW and an aperiodic hyperbolic secant function, especially as $A_s \to 2A$, Ω_I tends to zero. This means that the expression (12) can be regarded as an initial condition with a small aperiodic (simple peak) perturbation of background, which differs from the superposition of a CW and a periodic perturbation in the expression (11). Here we make use of the expression (12) as an initial condition to investigate the excitation of the Peregrine rogue wave. Similarly, the numerical simulations show that the evolution of the exact solution (7) can be well described by the initial condition (12) except for a translation.

Figure 6 shows the evolutions of the numerical solution of Eq. (2) with the initial condition (12) and the comparisons of the intensity profile of numerical and exact Peregrine rogue waves at peak position for $\alpha_3 = 0$ and $\alpha_3 \neq 0$, respectively. From it, one can see that the initial condition (12) evolves into a near-ideal Peregrine rogue wave, which differs from that shown in Figs. 5(a) and 5(b). Similarly, Figs. 6(a) and 6(b) show the breakup of the Peregrine rogue wave for long distance, which implies that the Peregrine rogue wave is unstable.

Comparing results in Fig. 5 and Fig. 6, we find that a small localized (single peak) perturbation pulse of CW background can excite a Peregrine rogue wave. Indeed, every peak in the initial expression (11) can excite a Peregrine rogue wave, thus a periodic perturbation of background resulted in the generation of a string of the Peregrine rogue waves, as shown in Figs. 5(a) and 5(b). So we can suggest that the Peregrine rogue wave can be excited by the interaction between the CW and a small localized (single peak) perturbation pulse. As an example, we consider a simple initial condition with Gaussian-type

perturbation pulse as follows

$$q(0,t) = A + \epsilon \exp(-\sigma t^2), \tag{13}$$

where ϵ is a modulation amplitude and a small quantity. The numerical simulations show that when the width of the initial perturbation pulse is wider enough, i. e. the parameter σ is smaller enough, the Peregrine rogue wave can be excited by the initial condition (13) even for nonintegrable HNLS equation (1). Figure 7 shows the evolution plots of the numerical solution for Eq. (1) with the initial condition (13), in which includes a numerical evolution of the initial condition (13) under nonintegrable case, as shown in Fig. 7(c). From Fig. 7(d), one can see that the main characteristics of the Peregrine rogue wave is kept. Certainly, the Peregrine rogue wave is unstable. This result can be used to understand the extreme localized events in ocean.

IV. THE INFLUENCE OF THE SELF-FREQUENCY SHIFT TO THE DYNAMICS OF THE PEREGRINE ROGUE WAVE

It should be noted that the equation (1) have not included the self-frequency shift effect arising from stimulated Raman scattering because the parameter α_5 is a real number. In the Section, we will discuss the influence of the self-frequency shift effect to the dynamics of the Peregrine rogue wave. In this case, the model governing pulse propagation can be written as [43]

$$\begin{aligned}\frac{\partial Q}{\partial \xi} = &-i\frac{\beta_2}{2}\frac{\partial^2 Q}{\partial \tau^2} + i\gamma|Q|^2 Q + \frac{\beta_3}{6}\frac{\partial^3 Q}{\partial \tau^3} \\ &- \frac{\gamma}{\omega_0}\frac{\partial |Q|^2 Q}{\partial \tau} - i\gamma T_R Q\frac{\partial |Q|^2}{\partial \tau},\end{aligned} \tag{14}$$

where τ and ξ represent the temporal coordinate and the propagation distance, β_2 is the group velocity dispersion, β_3 is the third-order dispersion, γ is the nonlinear coefficient of the fiber, and T_R is the Raman time constant. By introducing the dimensionless transformations $Q(\xi,\tau) = \sqrt{P_0}q(z,t)$, $t = \tau/T_0$, and $z = \xi/L_D$ with the dispersion length $L_D = T_0^2/|\beta_2|$, Eq. (14) becomes the form of Eq. (1) with the coefficients $\alpha_1 = -\beta_2/(2\,|\beta_2|)$, $\alpha_2 = \gamma L_D P_0$, $\alpha_3 = \beta_3 L_D/(6T_0^3)$, $\alpha_4 = -\gamma L_D P_0/(\omega_0 T_0)$ and $\alpha_5 = -i\gamma T_R L_D P_0/T_0$, respectively. It should be pointed out that here α_5 is a complex number, which describes the self-frequency shift effect arising from stimulated Raman scattering.

As an example, here we use realistic parameters for a highly nonlinear fiber at 1550nm with the group velocity dispersion $\beta_2 = -8.85 \times 10^{-1}$ ps^2/km, the third-order dispersion $\beta_3 = 1.331 \times 10^{-2}$ ps^3/km, and the nonlinear parameter $\gamma = 10$ W^{-1}·km^{-1} [28]. Thus, for a given initial power P_0, the parameters α_1, α_2, α_3, α_4 and α_5 can be determined. Note that in our simulations we take $\alpha_2 = 1$ by choosing a temporal scale $T_0 = [|\beta_2|/(\gamma P_0)]^{1/2}$, and the Raman time constant $T_R = 5$fs when the self-frequency shift is considered. We still take Eq. (13) as the initial condition, in which the realistic width of the initial perturbation pulse is $T_1 \equiv T_0/\sqrt{2\sigma}$.

Figure 8 presents the numerical evolution plots of the initial condition (13) with the initial perturbation pulse width $T_1 = 2$ps for the different initial power P_0. From Fig. 8, it can be seen that, in the absence of the self-frequency shift effect ($T_R = 0$), the Peregrine rogue wave in turn splits into two subpulses, three subpulses and so on, and can split into more subpulses for higher initial power, as shown in Figs. 8(a) and 8(b). These results are similar to the pulse splitting induced by higher-order modulation instability based on NLS equation in Ref. [22], but here the complex splitting dynamic evolutions are excited by a linear superposition of the CW and a small localized (single peak) perturbation pulse, and the higher-order effects, such as the third-order dispersion and the self-steepening, are included. However, when the self-frequency shift effect is considered, such splitting of the Peregrine rogue wave no longer appears, as shown in Figs. 8(c) and 8(d). It is surprising that, in this case, the dynamics of the Peregrine rogue wave mainly exhibits a peak changing propagation characteristic of the field amplitude except for some of small radiations, and has an increasing in peaking value, as shown in Figs. 8(e) and 8(f). This property can be used to the generation of the higher peak power pulse.

Furthermore, the dependences of the peak position $\xi_{\rm peak}$ of the excited Peregrine rogue wave on the modulation amplitude ϵ are considered, as shown in Fig. 9. From it one can see that for a given initial perturbation pulse width T_1 or initial power P_0, the peak position $\xi_{\rm peak}$ of the excited Peregrine rogue wave is a decreasing function of the modulation amplitude ϵ. Thus one can control the position of the excited Peregrine rogue wave by choosing suitably the initial perturbation pulse width or the initial power. Also, we find that the self-frequency shift effect do not influence the peak position $\xi_{\rm peak}$ of the excited Peregrine rogue wave.

V. CONCLUSIONS

In summary, based on the soliton solution on a CW background for integrable Hirota equation, we have presented the reduction mechanism and the main characteristics of the Peregrine rogue wave in the propagation of femtosecond pulses of optical fiber. The results have shown that there exist two processes of the formation of the Peregrine rogue wave, one is the reduction of CW→AB→PS, which is the localized process of CW background, other is the reduction of bright soliton→KMS→PS, which is the reduction process of the periodization of the bright soliton. The characteristics of the Peregrine rogue wave has been exhibited by strong temporal and spatial localization. Also, the initial excitations of the Peregrine rogue wave have been discussed.

The results have shown that a Peregrine rogue wave can be excited by a small localized (single peak) perturbation pulse of CW background, even for the nonintegrable HNLS equation. This means that the Peregrine rogue wave is a result of interaction between the continuous wave background and soliton. Furthermore, the numerical simulations have shown the Peregrine rogue wave is unstable. Finally, through the study for a realistic highly nonlinear fiber, it has been found that the self-frequency shift influences the dynamics of the Peregrine rogue wave. The results shown that, in the absence of the self-frequency shift, the Peregrine rogue wave can splits into several subpusles, however, when the self-frequency shift is considered, the Peregrine rogue wave no longer splits, and exhibits mainly a peak changing and increasing propagation property.

This research is supported by the National Natural Science Foundation of China grant 61078079, and the Shanxi Scholarship Council of China grant 2011-010.

[1] C. Kharif, E. Pelinovsky, and A. Slunyaev, *Rogue Waves in the Ocean*, (Springer, Heidelberg, 2009).
[2] C. Kharif and E. Pelinovsky, Eur. J. Mech. BFluids **22**, 603 (2003).
[3] A. Slunyaev, Eur. J. Mech. BFluids **25**, 621 (2006).
[4] V. E. Zakharov, A. I. Dyachenko, and A. O. Prokofiev, Eur. J. Mech. BFluids **25**, 677 (2006).
[5] V. P. Ruban, Phys. Rev. Lett. **99**, 044502 (2007).
[6] Andonowati, N. Karjanto, and E. van Groesen, App. Math. Mod **31**, 1425 (2007).
[7] D. R. Solli, C. Ropers, P. Koonath, and B. Jalali, Nature (London) **450**, 1054 (2007).
[8] A. N. Ganshin, V. B. Efimov, G.V. Kolmakov, L. P. Mezhov-Deglin, and P.V. E. McClintock, Phys. Rev. Lett. **101**, 065303 (2008).
[9] M. Shats, H. Punzmann, and H. Xia, Phys. Rev. Lett. **104**, 104503 (2010).
[10] J. Dudley, G. Genty, and B. Eggelton, Opt. Express **16**, 3644 (2008).
[11] D. R. Solli, C. Ropers, and B. Jalali, Phys. Rev. Lett. **101**, 233902 (2008).
[12] A. Mussot, A. Kudlinski, M. Kolobov, E. Louvergneaux, M. Douay and M. Taki, Opt. Express **17**, 17010 (2010).
[13] M. Taki, A. Mussot, A. Kudlinski, E. Louvergneaux, M. Kolobov, and M. Douay, Phys. Lett. A **374**, 691 (2010).
[14] A. R. Osborne, M. Onorato, and M. Serio, Phys. Lett. A **275**, 386 (2000).
[15] A. R. Osborne, Mar. Struct. **14**, 275 (2001).
[16] N. Akhmediev, A. Ankiewicz, and M. Taki, Phys. Lett. A **373**, 675 (2009).
[17] N. Akhmediev, J. M.Soto-Crespo, and A. Ankiewicz, Phys. Lett. A **373**, 2137 (2009).
[18] A. Ankiewicz, N. Devine, and N. Akhmediev, Phys. Lett. A **373**, 3997 (2009).
[19] N. Akhmediev, J. M. Soto-Crespo, and A. Ankiewicz, Phys. Rev. A **80**, 043818 (2009).
[20] N. Akhmediev, A. Ankiewicz, and J. M. Soto-Crespo, Phys. Rev. E **80**, 026601 (2009).
[21] Zhenya Yan, Phys. Lett. A **374**, 672 (2010).
[22] M. Erkintalo, K. Hammani, B. Kibler, Ch. Finot, N. Akhmediev, J. M. Dudley, and G. Genty, Phys. Rev. Lett. **107**, 253901 (2011).
[23] B. Kibler, K. Hammani, C. Michel, Ch. Finot, A. Picozzi, Phys. Lett. A **375**, 3149 (2011).
[24] D. H. Peregrine, J. Austral. Math. Soc. Ser. B**25**, 16 (1983).
[25] E. A. Kuznetsov, Sov. Phys. Dokl. **22**, 507 (1977).
[26] Ya. C. Ma, Stud. Appl. Math. **60**, 43 (1979).
[27] N. Akhmediev and V. I. Korneev, Theor. Math. Phys. **69**, 1089 (1986).
[28] B. Kibler, J. Fatome, C. Finot, G. Millot, F. Dias, G. Genty, N. Akhmediev, and J. M. Dudley, Nature Physics **6**, 790 (2010).
[29] K. Hammani, B. Kibler, C. Finot, Ph. Morin, J. Fatome, J. M. Dudley, and G. Millot, Opt. Lett. **36**, 112 (2011).
[30] Y. Kodama and A. Hasegawa, IEEE J. Quantum Electron. **23**, 510 (1987).
[31] R. Hirota, J. Math. Phys. **14**, 805 (1973) .
[32] M. Lakshmanan and S. Ganesan, J. Phys. Soc. Jpn. **52**, 4031 (1983).
[33] D. Mihalache, L. Torner, F. Moldoveanu, N.-C. Panoiu, and N. Truta, Phys. Rev. E **48**, 4699 (1993).
[34] D. Mihalache, N.-C. Panoiu, F. Moldoveanu, and D.-M. Baboiu, J. Phys. A: Math. Gen. **27**, 6177 (1994).
[35] K. Porsezian and K. Nakkeeran, Phys. Rev. Lett. **76**, 3955 (1996).
[36] D. Mihalache, N. Truta, and L. C. Crasovan, Phys. Rev. E **56**, 1064 (1997).
[37] L. Li, Z. H. Li, Z. Y. Xu, G. S. Zhou, and K. H. Spatscheck, Phys. Rev. E **66**, 046616 (2002).
[38] Z. Y. Xu, L. Li, Z. H. Li, and G. S. Zhou, Phys. Rev. E **67**, 026603 (2003).
[39] S. Q. Li, L. Li, Z. H. Li, and G. S. Zhou, J. Opt. Soc. Am. B **21**, 2089 (2004).
[40] A. Ankiewicz, J. M. Soto-Crespo, and N. Akhmediev, Phys. Rev. E **81**, 046602 (2010).
[41] Q. H. Park and H. J. Shin, Phys. Rev. Lett. **82**, 4432 (1999).
[42] M. J. Ablowitz, and P. A. Clarkson, *Soliton, Nonlinear Evolution Equations and Inverse Scattering* (University Press, Cambridge, 1991).
[43] G. P. Agrawal, *Nonlinear Fiber Optics* (Academic Press, New York, 1995).

Figures

FIG. 1: (Color online) The reduction process from the solution (3) to the Peregrine solution (4) as $(A_s, \omega_s) \to (2A^{\mp}, \omega)$. ($a^-$) $A_s = A$, $\omega_s = 0.6\omega$; (b^-) $A_s = 1.45A$, $\omega_s = 0.7\omega$; (c^-) $A_s = 1.6A$, $\omega_s = 0.8\omega$; (d^-) $A_s = 1.99A$, $\omega_s = 0.85\omega$; (a^+) $A_s = 3A$, $\omega_s = 1.4\omega$; (b^+) $A_s = 2.5A$, $\omega_s = 1.3\omega$; (c^+) $A_s = 2.4A$, $\omega_s = 1.2\omega$; (d^+) $A_s = 2.01A$, $\omega_s = 1.15\omega$; and (e) the Peregrine solution given by (4) with $A_s = 2A$ and $\omega_s = \omega$. The slope of red dashed lines is K_φ, and black solid lines is K_θ. Here the parameters are $A = 1$, $\omega = 1$, $t_0 = 0$, $z_0 = 5$, $\mu = 1$, $\alpha_1 = 0.5$, and $\alpha_3 = 0.05$.

FIG. 2: (Color online) The contour plots of (a) K_θ and (b) K_φ as a function of A_s and ω_s, where the parameters are $A = 1$, $\omega = 1$, $\mu = 1$, $\alpha_1 = 0.5$, and $\alpha_3 = 0.05$, and the contour values (from left to right) are 0.02, 0.1, 0.2, 0.3, 0.4, 0.5, 0.6, 0.7, 0.9, 1.1, 1.3 in (a), and the contour values are 1.1, 1.2, 1.4, 1.8, 3, −2.5, −0.9, −0.4, −0.2, −0.1 in (b), respectively.

FIG. 3: (Color online) (a) and (c) The evolution plots of the solutions (5) and (7), respectively, where the parameters are the same as in Fig. 1 except for $A_s = 1.5A$ in (a) and $A_s = 2.5A$ in (c); (b) and (d) The dependences of the ratio $t_{\rm per}/\delta t_0$ and $z_{\rm per}/\delta z_0$ on A_s/A, respectively.

FIG. 4: (Color online) The evolution plots of the Peregrine solution given by Eq. (4) for $\alpha_3 = 0$ in (a) and $\alpha_3 = 0.2$ in (b), respectively; (c) The distribution of the light intensity against the CW background given by Eq. (9) at $z = z_0$; (d) The evolutions of the energy exchange between the PS and the CW background for the different TOD parameters. Here the parameters are $A = 1$, $\omega = 1$, $t_0 = 0$, $z_0 = 5$, $\mu = 1$, and $\alpha_1 = 0.5$.

FIG. 5: (Color online) The evolution plots of the numerical solution of Eq. (2) with the initial condition (11) and the comparisons of the intensity profiles of numerical and exact results at peak position, respectively. (a) and (c) $\alpha_3 = 0$, (b) and (d) $\alpha_3 = 0.2$. Note that in (c) and (d), the blue dotted curves are the exact results given by Eq. (4) at $z = z_0$ and the black solid curves are the numerical results at $z = 5.9$ in (a) and $z = 5.2$ in (b) [the white dotted lines in (a) and (b)], respectively. Here $A_s = 1.95$, and other parameters are the same as in Fig. 4.

FIG. 6: (Color online) The evolution plots of the numerical solution of Eq. (2) with the initial condition (12) and the comparisons of the corresponding intensity profile at peak position, respectively. (a) and (c) $\alpha_3 = 0$, (b) and (d) $\alpha_3 = 0.2$. Note that in (c) and (d), the blue dotted curves are the exact results given by Eq. (4) at $z = z_0$ and the black solid curves are the numerical results at $z = 10.2$ in (a) and $z = 6.4$ in (b) [the white dotted lines in (a) and (b)], respectively. Here $A_s = 2.05$, $\omega = 0.5$, and other parameters are the same as in Fig. 4.

FIG. 7: (Color online) The numerical evolution plots of the initial condition (13). (a) for NLS equation with $\alpha_3 = 0$; (b) for Hirota equation (2) with $\alpha_3 = 0.1$; (c) for HNLS equation (1) with $\alpha_3 = 0.05$, $\alpha_4 = 0.285$ and $\alpha_5 = -0.315$, and (d) the distributions of the intensity profile at $z = 6.975$ in (a), $z = 6.825$ in (b) and $z = 6.9$ in (c). Here $\alpha_1 = 0.5$, $A = 1$, $\epsilon = 0.05$ and $\sigma = 0.05$.

FIG. 8: (Color online) The numerical evolution plots of the initial condition (13) for the different initial power. Here (a) and (b) the absence of self-frequency shift ($T_R = 0$); (c) and (d) the presence of self-frequency shift ($T_R = 5$fs), and (e) and (f) the corresponding power density distributions at the different distance labeled by the white dotted lines in (b) and (c), respectively. In (a), (c) and (e), the initial power $P_0 = 0.3$W, and in (b), (d) and (f), the initial power $P_0 = 0.4$W. Here $\epsilon = 0.2$ and $A = 1$.

FIG. 9: (Color online) The dependences of the peak position $\xi_{\rm peak}$ of the excited Peregrine rogue wave on the modulation amplitude ϵ for (a) the different initial power and a given initial perturbation pulse width $T_1 = 2$ps, and (b) the different initial perturbation pulse width T_1 and a given initial power $P_0 = 0.4$W. Here the solid, dashed and dotted curves correspond to the results of $T_R = 0$, and the open diamonds, circles and triangles correpond to the results of $T_R = 5$fs, and the parameter $A = 1$.

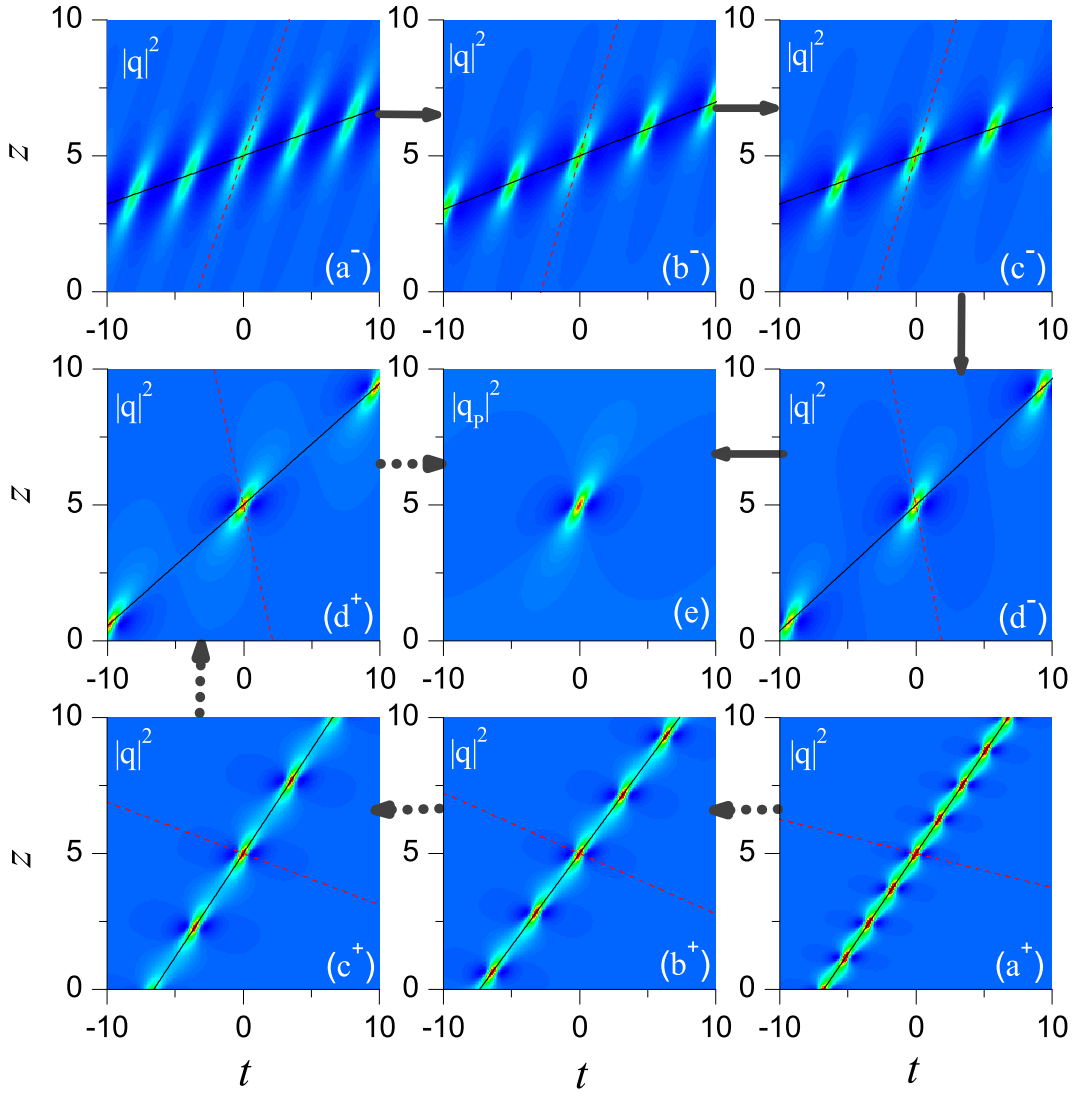

Figure 1 AK10952E 27Mar2012

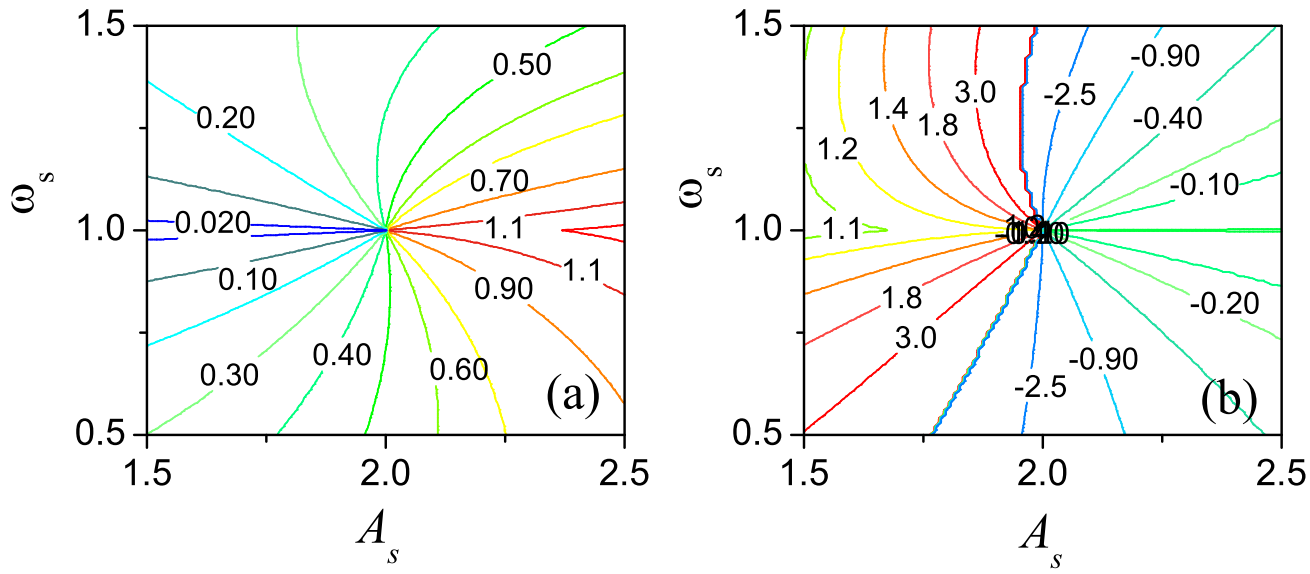

Figure 2 AK10952E 27Mar2012

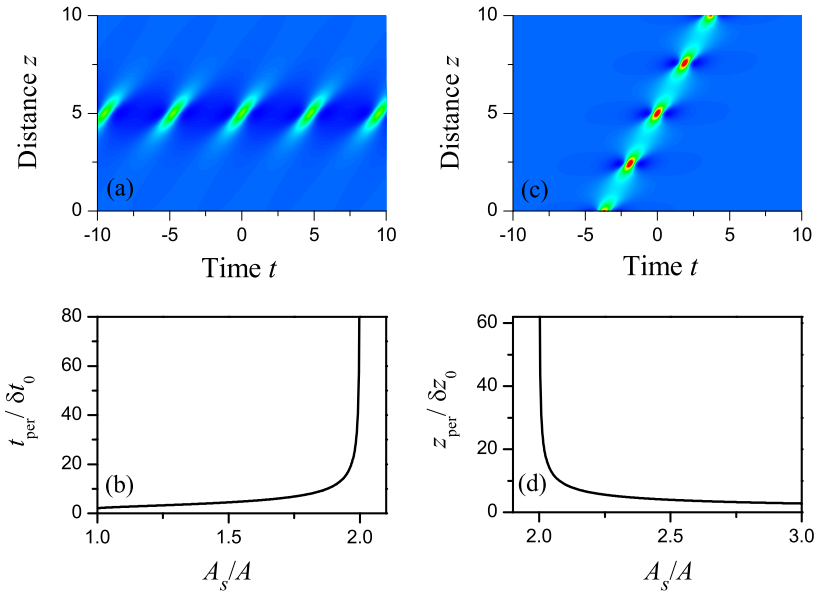

Figure 3 AK10952E 27Mar2012

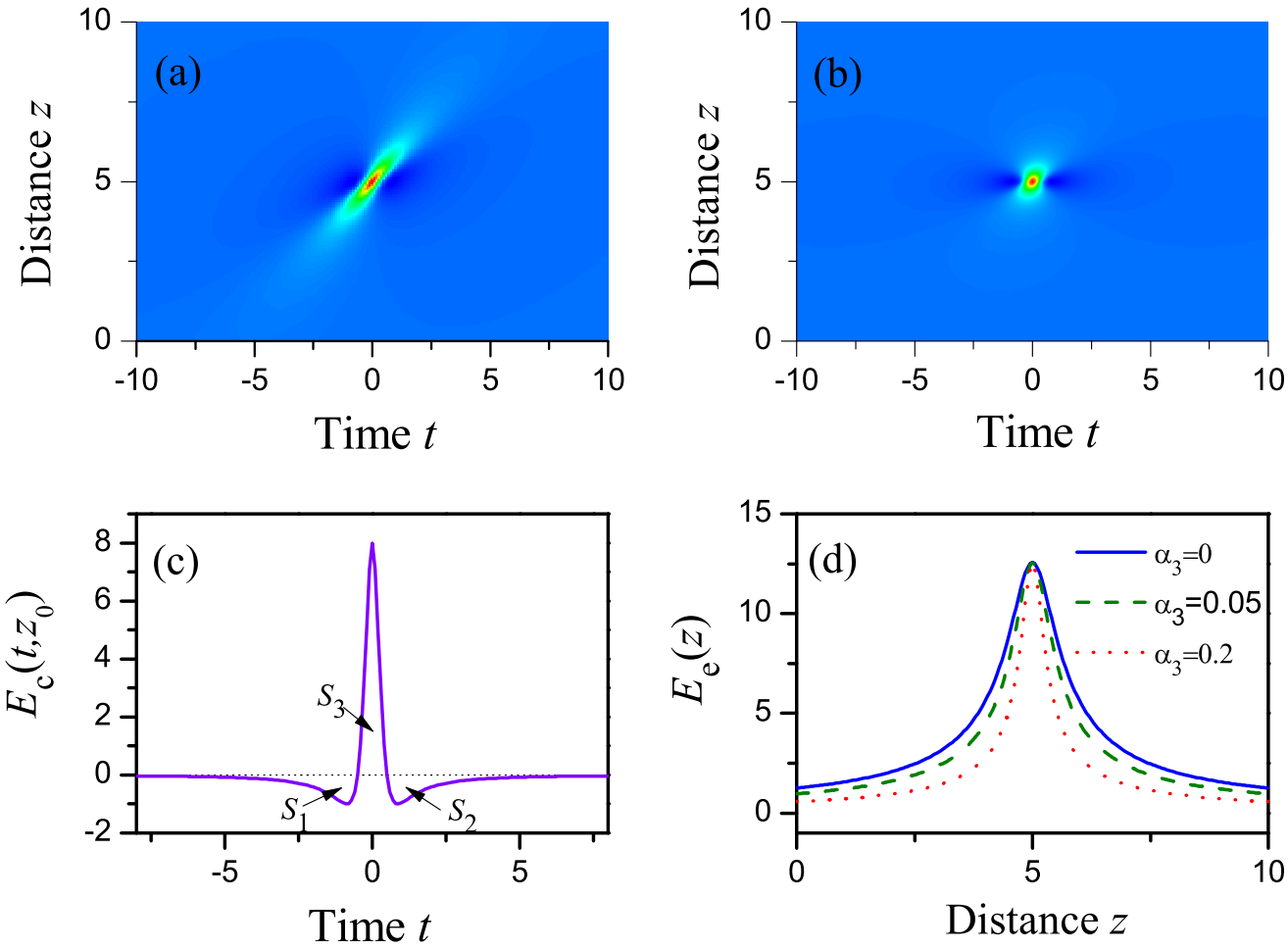

Figure 4 AK10952E 27Mar2012

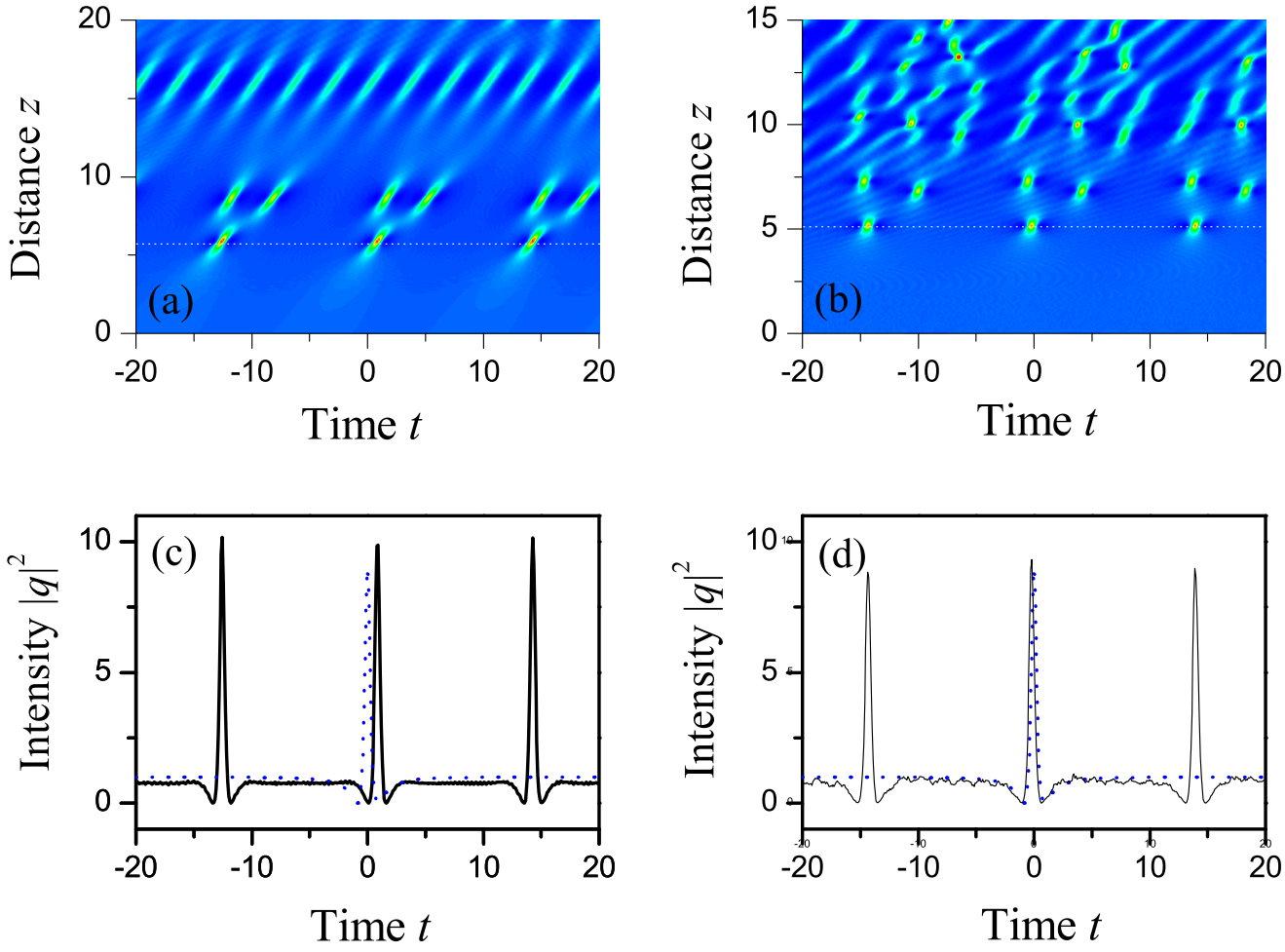

Figure 5 AK10952E 27Mar2012

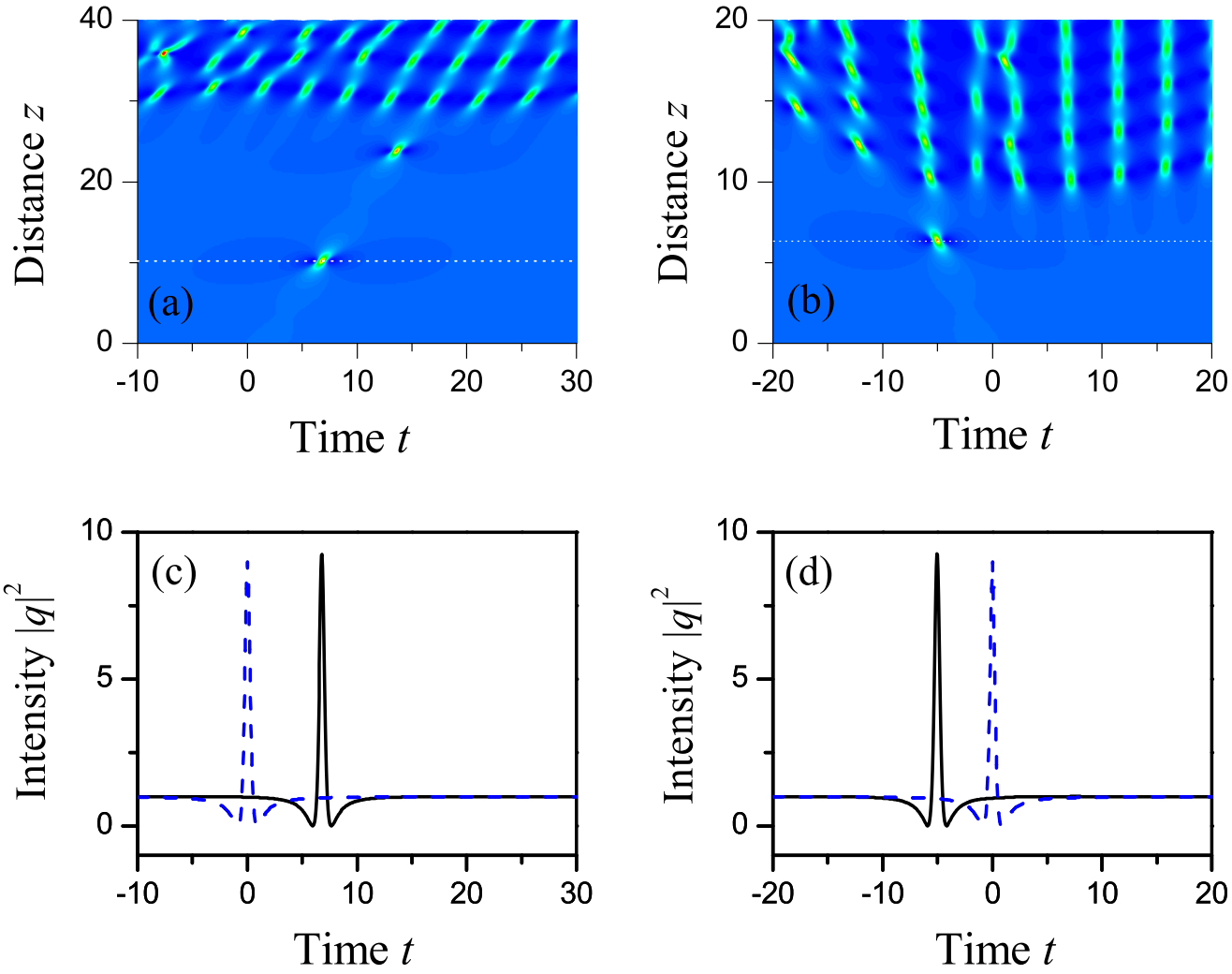

Figure 6 AK10952E 27Mar2012

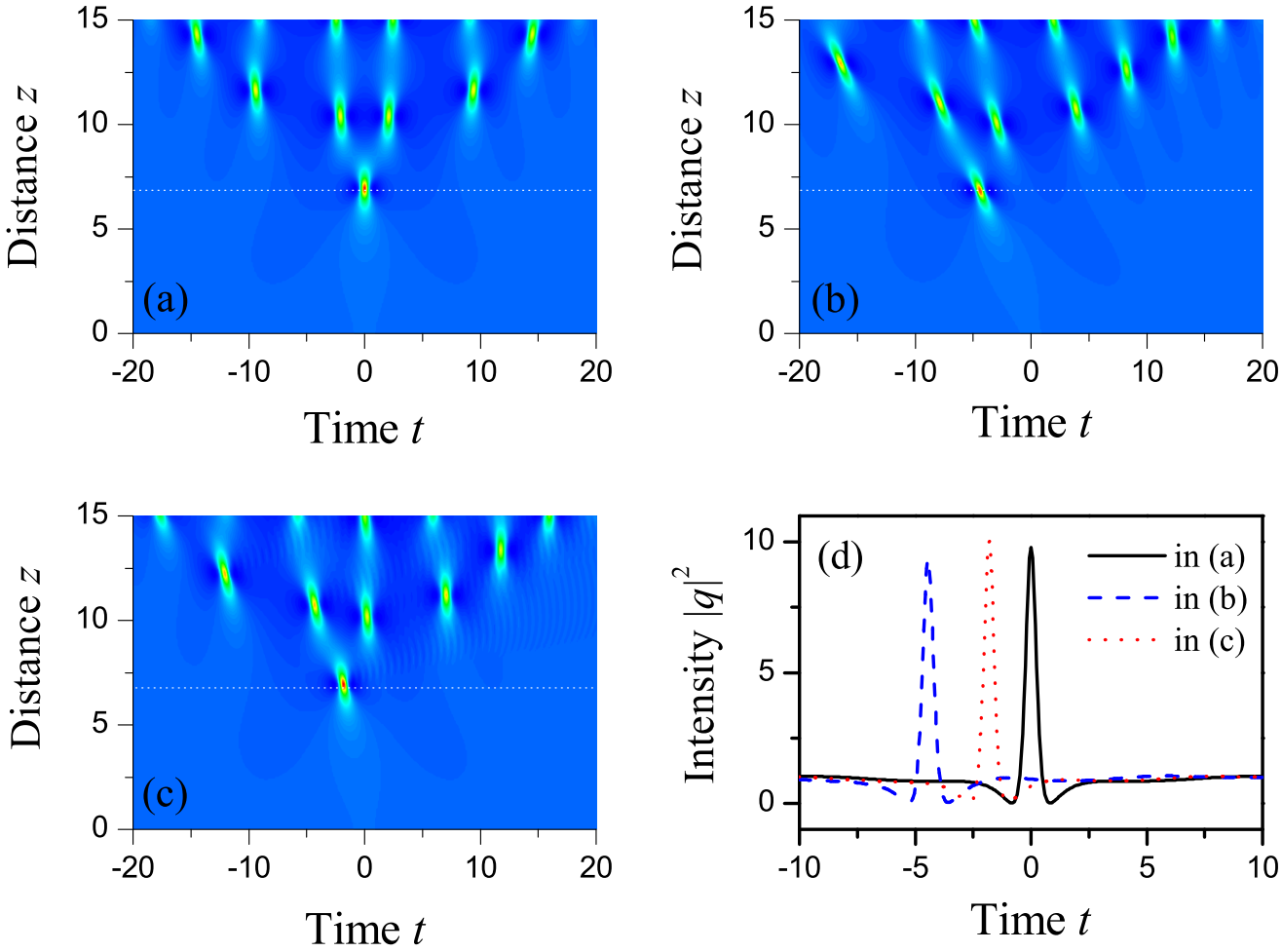

Figure 7 AK10952E 27Mar2012

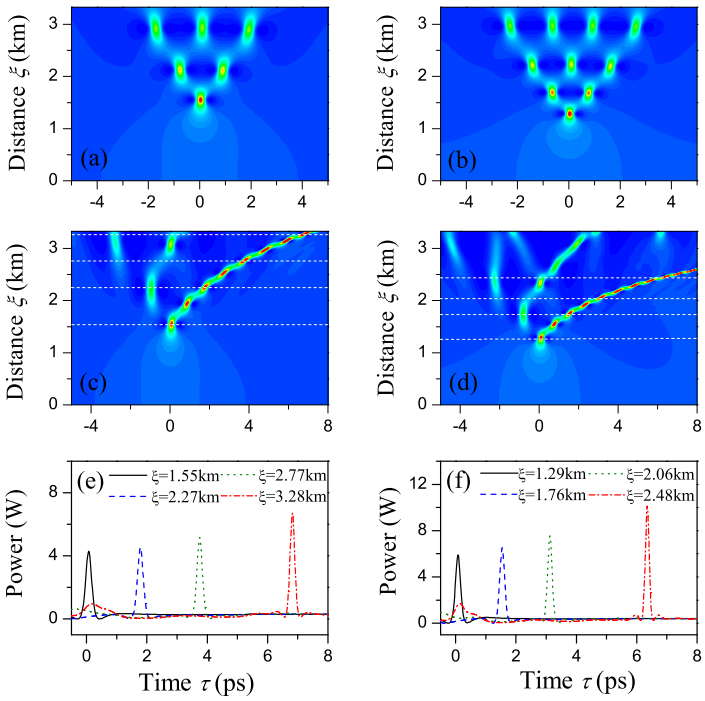

Figure 8 AK10952E 27Mar2012

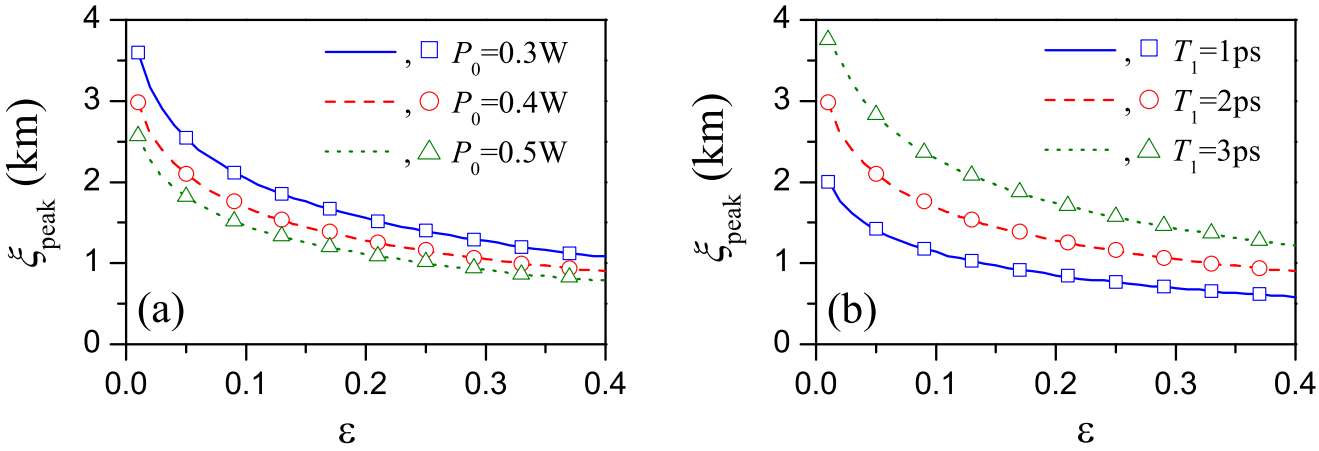

Figure 9 AK10952E 27Mar2012